# Flagellar targeting of an arginine kinase requires a conserved lipidated protein intraflagellar transport (LIFT) pathway in *Trypanosoma brucei*

Received for publication, May 8, 2020, and in revised form, June 18, 2020 Published, Papers in Press, June 25, 2020, DOI 10.1074/jbc.RA120.014287

**Maneesha Pandey, Yameng Huang (黄 亚檬), Teck Kwang Lim, Qingsong Lin, and Cynthia Y. He***

*From the Department of Biological Sciences, National University of Singapore, Singapore*

Edited by Enrique M. De La Cruz

**Both intraflagellar transport (IFT) and lipidated protein intraflagellar transport (LIFT) pathways are essential for cilia/flagella biogenesis, motility, and sensory functions. In the LIFT pathway, lipidated cargoes are transported into the cilia through the coordinated actions of cargo carrier proteins such as Unc119 or PDE6δ, as well as small GTPases Arl13b and Arl3 in the cilium. Our previous studies have revealed a single Arl13b ortholog in the evolutionarily divergent *Trypanosoma brucei*, the causative agent of African sleeping sickness. TbArl113 catalyzes two TbArl3 homologs, TbArl3A and TbArl3C, suggesting the presence of a conserved LIFT pathway in these protozoan parasites. Only a single homolog to the cargo carrier protein Unc119 has been identified in *T. brucei* genome, but its function in lipidated protein transport has not been characterized. In this study, we exploited the proximity-based biotinylation approach to identify binding partners of TbUnc119. We showed that TbUnc119 binds to a flagellar arginine kinase TbAK3 in a myristoylation-dependent manner and is responsible for its targeting to and enrichment in the flagellum. Interestingly, only TbArl3A, but not TbArl3C interacted with TbUnc119 in a GTP-dependent manner, suggesting functional specialization of Arl3-GTPases in *T. brucei*. These results establish the function of TbUnc119 as a myristoylated cargo carrier and support the presence of a conserved LIFT pathway in *T. brucei*.**

Cilia or eukaryotic flagella are present in eukaryotic organisms ranging from protists, invertebrates to vertebrates. Depending on their structure and protein compositions, cilia and flagella can perform sensory functions or impart motility. Ciliary mutations and malfunctioning have been implicated in many diseases collectively known as ciliopathies (1).

Ciliary proteins are synthesized in the cytosol and trafficked to the ciliary compartment by two main pathways, the intraflagellar transport (IFT) and the lipidated protein intraflagellar transport (LIFT) (1, 2). IFT has been extensively characterized with well-documented functions in anterograde and retrograde transport of ciliary structural components (3–7). LIFT, on the other hand, has recently emerged as a parallel trafficking pathway dedicated to lipidated cargoes associated with ciliary membrane (8–11). Only a few lipidated proteins have been identified as LIFT cargoes, and most of these proteins are important for ciliary signaling functions (10–12).

In mammals, LIFT comprises of small GTPases Arl13b and Arl3, Arl3-GTPase activating protein RP2, as well as carrier proteins phosphodiesterase 6δ (PDE6δ) and Unc119 paralogs (2). PDE6δ or Unc119 binds to lipidated cargoes synthesized in the cytosol and facilitates their import into the ciliary lumen. Arl13b is enriched in the cilia, where it acts as a guanine nucleotide exchange factor (GEF) on Arl3 (8). Activated, GTP-bound Arl3 can bind to PDE6δ or Unc119, and functions as a displacement factor to release lipidated cargoes associated with the carrier proteins inside of the ciliary lumen (13–15). Arl3-GTP hydrolysis is then catalyzed by RP2 at the base of the cilium, where Arl3-GDP dissociates from the carrier proteins (16).

PDE6δ and Unc119 paralogs contain a conserved phosphodiesterase domain, which is crucial for interaction with lipidated cargoes (17). PDE6δ binds ciliary farnesylated proteins such as inositol polyphosphate 5′-phosphatase E (INPP5E) (12) and is required for its ciliary targeting. PDE6δ also interacts with nonciliary cargoes such as prenylated RAS-GTPases and affects their membrane distribution and signalling functions (18). Unc119 paralogs Unc119A and Unc119B share 60% sequence homology and both carry myristoylated proteins into the cilia (17). Only a few myristoylated cargoes have been identified (10), and Nephrocystin-3 (NPHP3) is the only ciliary cargo identified to date that interacts with both Unc119A and Unc119B (11). Like PDE6δ, Unc119A has also been shown to have nonciliary functions via interactions with Src-type tyrosine kinases Lyn (19), Fyn (20), and Lck as well as Rab11 (21, 22) and Dynamin GTPases (23), all of which have predicted *N*-myristoylation sites. Through these interactions, Unc119A influences the distribution and signaling functions of these proteins.

The function of Unc119 has also been extensively characterized in *Caenorhabditis elegans,* where it is also a lipid-binding protein required for G protein trafficking in sensory neurons (24). Additionally, a recent study has shown that *C. elegans* Unc119 interacts with both Arl3 and Arl13, stabilizing the interaction between Arl3 and Arl13, and facilitating GTP activation of Arl3 (25). Importantly, *C. elegans* Unc119 binds to Arl3 independent of its GTP-bound state, making Unc119 an unlikely effector of Arl3-GTP. The *C. elegans* Unc119 thus functions differently to its mammalian counterparts, which may represent functional differences in evolutionarily divergent ciliated organisms (25).

*Trypanosoma brucei*, causative agent of human African trypanosomiasis (sleeping sickness) as well as nagana in domestic

This article contains supporting information.

* For correspondence: Cynthia Y. He, dbshyc@nus.edu.sg.

animals, is a protozoan parasite belonging to the Kinetoplastid group, which are considered as one of the earliest-divergent eukaryotic organisms (26). *T. brucei* is also emerging as a useful model to understand flagellar structure, biogenesis, and functions (27). The flagellum of *T. brucei* has both signaling and motility functions and is crucial for the viability and pathogenesis of this parasite (28). Both IFT and LIFT pathway components have been identified in *T. brucei*. Although the function and regulation of the IFT pathway has been extensively characterized (7), the presence of a conserved LIFT pathway in *T. brucei* was only recently recognized. A single orthologue of Arl13b was found in *T. brucei* genome, with its protein product enriched in the flagellar axoneme via a Docking and Dimerization domain (29). Interestingly, *T. brucei* has three Arl3 homologs, namely TbArl3A (Tb927.3.3450), TbArl3B (Tb927.10.8580), and TbArl3C (Tb927.6.3650). TbArl13 interacts and catalyzes nucleotide exchange on both TbArl3A and TbArl3C, but not TbArl3B. Consistently, only TbArl3A and TbArl3C exhibit flagellar biogenesis effects upon overexpression of the GTP-locked mutants (29).

A single Unc119 ortholog (TbUnc119, Tb927.2.4580) was identified in an *in silico* screen of *T. brucei* genome (30). TbUnc119 is present in the flagellum, but depletion of TbUnc119 via tetracycline-inducible RNAi does not produce any observable effect on cell growth or motility (30). Thus, the cellular function of TbUnc119 is not known and its role in lipidated protein transport in *T. brucei* has not been studied. In this study we used BioID, a proximity-based biotinylation method (31, 32) to identify interacting partners of TbUnc119. Our results identified a flagellar arginine kinase TbAK3 as a TbUnc119 cargo. We also showed that TbArl3A but not TbArl3C binds to TbUnc119, emphasizing the functional difference between different TbArl3-GTPase isoforms in *T. brucei*.

## Results

### *Kinetoplastids contain a single Unc119 homolog*

*T. brucei* has a single Unc119 homolog (TbUnc119) encoded by Tb927.2.4580, which has been shown to be a flagellar protein in an earlier study (30). Phylogenetic analyses were then performed on TbUnc119 and Unc119/PDE6δ homologs identified in various model organisms (Fig. S1*A*). TbUnc119 formed a clad with other Unc119 homologs distinct from PDE6δ proteins. Unc119 is highly conserved among kinetoplastids (Fig. S1*B*). Notably, PDE6δ homologue could not be found despite extensive searches of the *T. brucei* genome. Further BLAST searches confirmed the absence of PDE6δ in all Kinetoplastid members and most single cellular eukaryotes we have examined, with the possible exception of *Paramecium tetraurelia* (33). Together these results suggest that Unc119 is likely the only conserved lipidated protein carrier belonging to the Unc119 supergene family (33) in *T. brucei* and other Kinetoplastid organisms.

The knockdown of TbUnc119 did not produce detectable growth defects in the insect-infectious procyclic form (PCF) cells (Fig. S2*A*), which corroborates the previous study (30). In the mammal infectious bloodstream form (BSF) *T. brucei*, a mild growth delay was consistently observed post TbUnc119-RNAi induction (Fig. S2*B*). No significant phenotypic changes were observed in the PCF or BSF cells. Taken together, these results confirmed that TbUnc119 is not essential for *T. brucei* cell survival or flagellar biogenesis in culture. These results are also consistent with the nonlethal mutant phenotypes of Unc119 orthologues previously reported in *C. elegans* (34) or zebrafish (35).

### *Identification of TbUnc119-interacting proteins by proximity-based biotinylation*

In both *C. elegans* and mammals, Unc119 is characterized as a cargo carrier/chaperone involved in intraflagellar transport of myristoylated ciliary proteins, and Unc119 association with the cargo is regulated by the Arl13b-Arl3 pathway (8, 11). The function of the LIFT pathway and its flagellar cargoes have never been examined in the evolutionarily divergent *T. brucei.* We therefore decided to revisit the function of TbUnc119, by investigating its interacting proteins.

We utilized the proximity-dependent biotinylation approach, using an improved version of biotin ligase BioID2 (31). The BioID2 tag was fused to either the N terminus (3HA-BioID2-TbUnc119) or the C terminus (TbUnc119-BioID2-HA) of TbUnc119 and expressed using a cumate-inducible expression system in the procyclic cells (36). Both 3HA-BioID2-TbUnc119 and TbUnc119-BioID2-HA cells showed strong labeling throughout the cytoplasm (Fig. S3), by anti-HA that stains the TbUnc119 fusions and streptavidin-Alexa Fluor 568 that stains the biotinylated products. Weak signal was also observed along the flagellum (Fig. S3, *B* and *C*, *arrowheads*). These results suggest both flagellar and cytoplasmic presence of TbUnc119 and its biotinylated products. Similar cytoplasmic presence is also apparent in cells with endogenous expression of mNeonGreen-tagged TbUnc119, either at the N or C terminus (Tryptag, Tb927.2.4580) (37). Biotinylated proteins from both 3HA-BioID2-TbUnc119 and TbUnc119-BioID2-HA cells were affinity purified (Fig. S3, *D* and *E*) and analyzed by LC-MS/MS. A total of 136 and 39 candidates from 3HA-BioID2-TbUnc119 and TbUnc119-BioID2-HA cells, respectively, were identified (Fig. 1*A*, Table S1). Among them, 28 high-confidence candidates were found in both 3HA-BioID2-TbUnc119 and TbUnc119-BioID2-HA cells (Fig. 1*B*, Table S2). It is not clear why 3HA-BioID2-TbUnc119 had more hits identified than TbUnc119-BioID2-HA cells. One possibility is that the position of the BioID2 tag at the C terminus of TbUnc119 may interfere with its interaction with other proteins.

A group of arginine kinases (TbAKs) and kinetoplastid membrane proteins, TbKMP-11, were found to top the list (Fig. 1*B*). Of the three highly similar TbAK proteins identified, only TbAK3 (encoded by Tb927.9.6210 (38); and named TbAK1 in another study (39)) contains a myristoylation consensus sequence. TbAK3 was also identified as a high-confidence candidate in a recent myristoylation proteomics study (40). Small myristoylated proteins (TbSMP1-1 encoded by Tb927.1.2230 and TbSMP1-2 by Tb927.1.2260), which also possess a consensus myristoylation sequence were identified in the 3HA-BioID2-TbUnc119 list. These kinetoplastid-specific proteins resemble calpain-like proteins and are associated with the cell

A

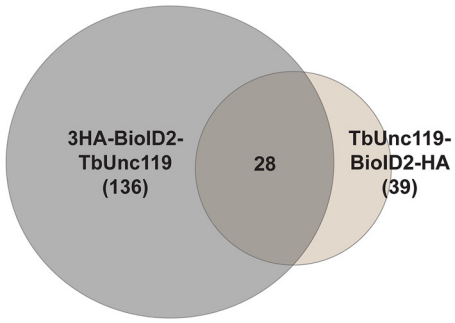


B

Selected TbUnc119-BioID candidates

| Accession | Protein content (%) | | Description | N-Myristoylation prediction (G2 or (MGXXXS/T) | Presence in Myristoylation proteome (Wright et al. 2016) |
|---|---|---|---|---|---|
| | 3HA-BioID2-TbUnc119 | TbUnc119-BioID2-HA | | | |
| Tb927.9.6210,Tb927.9.6230/50, Tb927.9.6290 | 2.67 | 2.33 | Arginine Kinase | Tb927.9.6210 only (**MG**FGS**S**) | Yes |
| Tb927.2.4580 | 2.48 | 1.44 | TbUnc119 | - | - |
| Tb927.9.13785, Tb927.9.13795, Tb927.9.13820, Tb927.9.13860, Tb927.9.13920 | 2.01 | 3.29 | Kinetoplastid membrane protein 11 (KMP11) | - | - |
| Tb927.3.4590 | 1.47 | 0.37 | Hypothetical protein | G2 | Yes |
| Tb927.6.3650 | 0.52 | ND | TbArl3C | - | - |
| Tb927.3.3450 | 0.31 | ND | TbArl3A | G2 | Yes |
| Tb927.6.1800 | 0.28 | 1.28 | Protein phosphatase 2C | G2 | Yes |
| Tb927.1.2230, Tb927.1.2260 | 0.14 | ND | Small myristoylated protein 1-1, 1-2 | **MG**CGG**S** | Yes |

**Figure 1. Proximity-dependent biotinylation screening for TbUnc119 interacting proteins.** *A,* a Venn diagram summarizing the MS results of two independent BioID experiments, one using cells stably expressing 3HA-BioID2-TbUnc119 with BioID2 fused to the N terminus of TbUnc119 and the other TbUnc119-BioID2-HA with BioID2 fused to the C terminus. *B,* list of selected BioID candidates. Protein candidates identified are ordered according to calculated protein content in the BioID experiment using 3HA-BioID2-TbUnc119 as the bait. Protein content of the candidates in the TbUnc119-BioID2-HA experiment is also shown wherever applicable. The description of the protein was obtained from the Kinetoplastid Genomics resource (www.tritrypdb.org). *ND*, not detected.

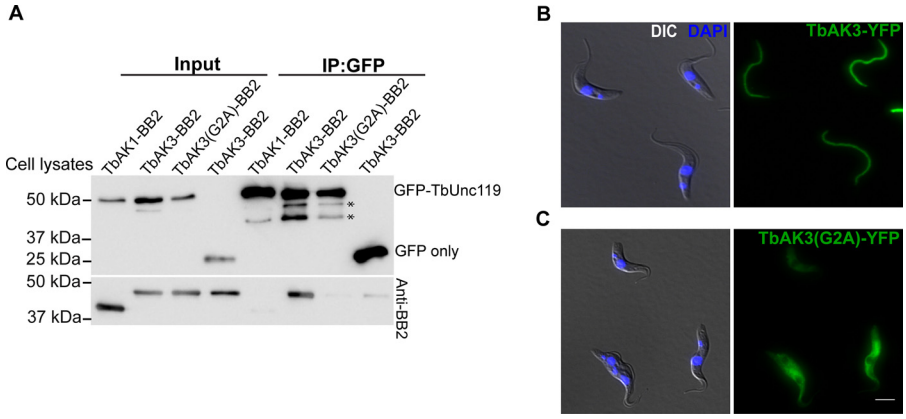


**Figure 2. Myristoylation of TbAK3 is critical for its flagellar targeting and its interaction with TbUnc119.** *A,* lysates of cells stably expressing GFP-TbUnc119 and TbAK1-BB2, TbAK3-BB2, or TbAK3(G2A)-BB2, respectively, were incubated with GFP-nAb beads. Proteins bound to the beads were fractionated on SDS-PAGE followed by immunoblotting with anti-GFP and anti-BB2 antibodies. Cells co-expressing GFP and TbAK3-BB2 were used as a negative control. *Asterisks* indicate possible degradation products of GFP-TbUnc119. *Input*: 3% of cell lysates. *B* and *C,* cells expressing TbAK3-YFP or TbAK3(G2A)-YFP were viewed after fixation with 4% PFA. Nuclear and kinetoplast DNA were stained with DAPI (*blue*). *Scale bar*, 5 $\mu$m.

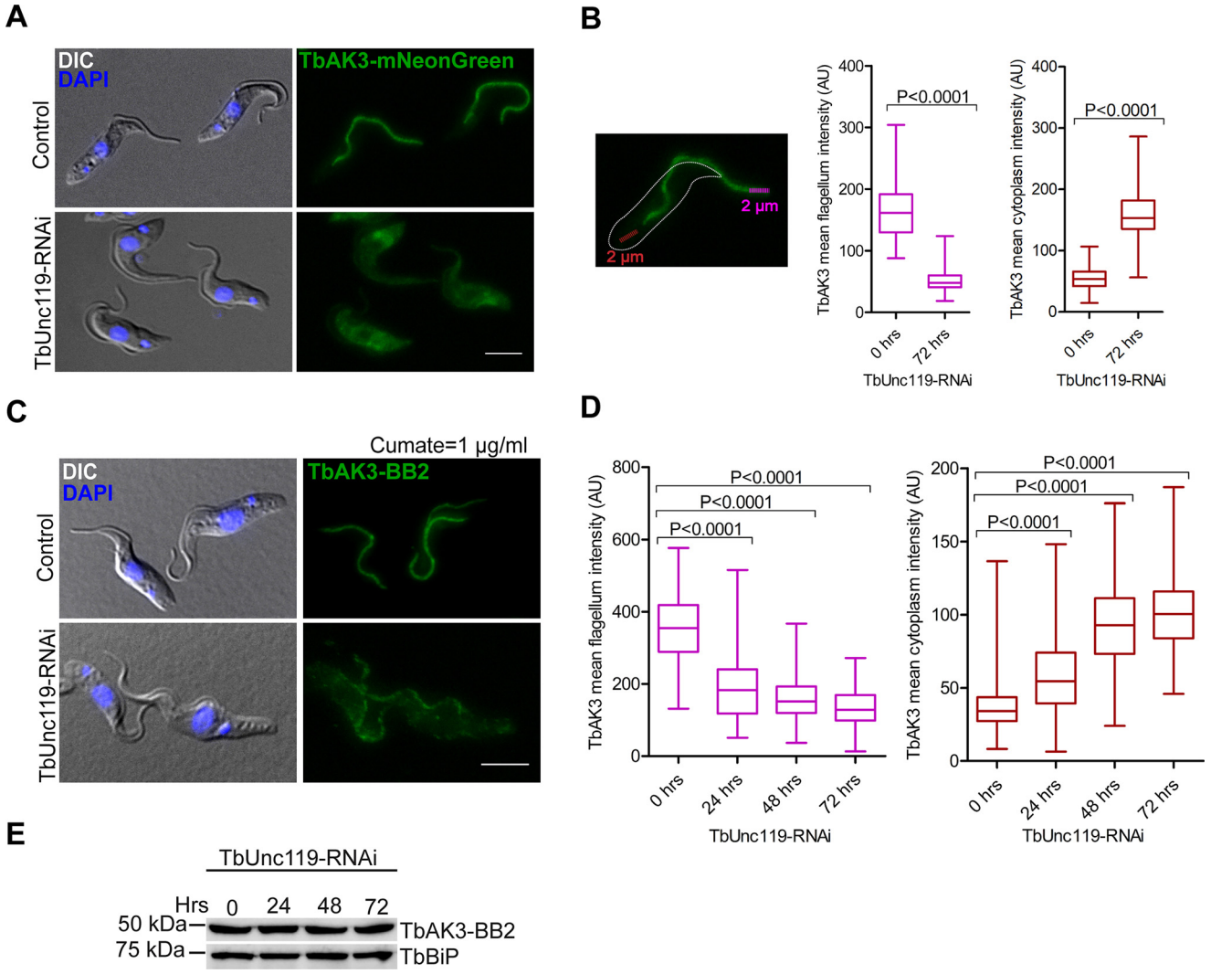


**Figure 3. Flagellar targeting of TbAK3 requires TbUnc119.** *A,* procyclic cells stably expressing TbAK3-mNeonGreen from an endogenous allele were induced for TbUnc119-RNAi. Control and induced cells were fixed with 4% PFA. *B,* TbAK3-mNeonGreen intensity in the flagellum and in the cytosol was measured using plot profile function as illustrated here and detailed under "Experimental procedures." Results are shown as *box plots*, with the whiskers marking the minimum and maximum values, the *box* showing the 25th to 75th percentiles and the *bars* in the *box* showing the median. $n > 150$ cells were measured for each condition at each time point. Two-tailed Student's *t* test was performed, and *p* values are indicated in the plots. *C–E,* cells containing tetracycline-inducible TbUnc119-RNAi and cumate-inducible TbAK3-BB2 expression were induced for TbUnc119-RNAi for 0, 24, or 48 h prior to induction of TbAK3-BB2 expression. The induction of TbAK3-BB2 expression was fixed at 1 $\mu$g/ml of cumate for 24 h to ensure similar expression levels in different experiments (*E*). Cells were then fixed and processed for immunostaining with anti-BB2 (*C*). Quantitation of the TbAK3-BB2 signal in the flagellum and the cytosol was performed as illustrated in *B*. $n > 100$ cells were measured for each condition at each time point (*D*). *Scale bar*, 5 $\mu$m.

membrane (41). TbArl3A and TbArl3C, both components of *T. brucei* flagellum with confirmed flagellar functions (29), were also identified in 3HA-BioID2-TbUnc119 BioID.

### *The flagellar targeting of TbAK3 requires TbUnc119*

Three arginine kinases are found in *T. brucei*, sharing 85–99% sequence identity (39) and thus could not be distinguished in the BioID MS results. TbAK1 (encoded by Tb927.9.6290) is localized throughout the cytoplasm; and TbAK2 (encoded by Tb927.9.6250) is associated with the glycosomes, a peroxisome-like organelle in *T. brucei* (39). TbAK3 (encoded by Tb927.9.6210) is present on the flagellar membrane and is the only TbAK that is myristoylated (39, 40, 42).

To test if TbAK3 interacted with TbUnc119, TbAK3 was fused to a small BB2 tag (43) at the C terminus and co-expressed with GFP-TbUnc119. Immunoprecipitation was then performed using GFP nAb-conjugated beads. TbAK3-BB2 co-immunoprecipitated with GFP-TbUnc119, but not GFP only (Fig. 2*A*). As another control, TbAK1-BB2 did not co-immunoprecipitate with GFP-TbUnc119, suggesting a specific interaction between TbAK3 and TbUnc119. The TbAK3-TbUnc119 interaction is myristoylation-dependent, as TbAK3 (G2A)-BB2 failed to co-immunoprecipitate with GFP-TbUnc119. The myristoylation mutation also disrupted the flagellar localization of TbAK3 (Fig. 2, *B* and *C*). Together these results indicate that the flagellar localization of TbAK3 and its interaction with TbUnc119 are both myristoylation-dependent.

Next we asked whether TbAK3 flagellar targeting required TbUnc119. We tagged one endogenous allele of TbAK3 with the fluorescent reporter mNeonGreen in the TbUnc119-RNAi cell line. In control cells, TbAK3-mNeonGreen was enriched in

the flagella with a weak signal in the cytosol (Fig. 3*A*). Upon TbUnc119-RNAi induction, the flagellum enrichment of TbAK3 diminished and an increased cytosolic signal was observed (Fig. 3, *A*, quantitated in *B*). To further establish the flagellar targeting dynamics of TbAK3, we generated a stable cell line with tetracycline-inducible TbUnc119-RNAi and cumate-inducible expression of TbAK3-BB2. The expression of TbAK3-BB2 was induced for a fixed period of 24 h, at different times post TbUnc119-RNAi induction. A gradual reduction in flagellar TbAK3 and an increase in the cytoplasmic TbAK3 was observed over the course of TbUnc119-RNAi (Fig. 3, *C*, quantitated *D*), despite similar expression levels of TbAK3 at different time points (Fig. 3*E*). These results suggested that the loss of TbUnc119 inhibited the entry of TbAK3 into the flagellum.

### *TbUnc119 binds to TbSMP1-1, but is not required for TbSMP1-1 intracellular distribution*

To address whether TbUnc119 may have nonciliary functions as observed with animal Unc119 orthologs, we examined TbUnc119-BioID candidates for nonciliary myristoylated proteins. The small myristoylated protein TbSMP1-1 (encoded by Tb927.1.2230) contains an N-terminal myristoylation site (G2) and is enriched at the cell membrane of *T. brucei* (41). The interaction between TbSMP1-1 and TbUnc119 was confirmed by co-immunoprecipitation (Fig. 4*A*). Although TbSMP1-1-GFP was enriched in the cell periphery consistent with plasma membrane association, TbSMP1-1(G2A)-GFP mutant lost cell membrane enrichment and was found throughout the cytosol (Fig. 4, *B* and *C*). This observation was further confirmed by profiling the fluorescent intensity across randomly selected TbSMP1-1-GFP and TbSMP1-1(G2A)-GFP expressing cells (Fig. 4, *B* and *C*). Silencing of TbUnc119, however, had no detectable effects on TbSMP1-1-GFP distribution in the cell (Fig. 4*D*).

### *TbUnc119 interacts specifically with TbArl3A in a GTP-dependent manner*

The best characterized function of Unc119 is in the context of the LIFT pathway as a carrier for myristoylated cargoes. Once the cargo-Unc119 complex is inside of the ciliary lumen, Arl3-GTP acts as a displacement factor, binds to Unc119, and releases the cargo (9, 11). Unlike vertebrates that contain only a single Arl3 protein, *T. brucei* has two Arl3 homologues, TbArl3A and TbArl3C, which are both associated with the flagellum and exhibit flagellar phenotypes when overexpressed as GTP-locked forms (29). Interestingly, both TbArl3A and TbArl3C were found in the TbUnc119 BioID screen, albeit only in the 3HA-BioID2-TbUnc119 cells.

To confirm the interaction of TbUnc119 with TbArl3-GTPases, co-immunoprecipitation assays were performed on cells stably expressing GFP-TbUnc119 and epitope-tagged TbArl3A or TbArl3C from an endogenous allele. TbArl3A-mNeonGreen-BB2 specifically co-precipitated with GFP-TbUnc119, but not with GFP only (Fig. 5*A*); TbArl3C-mNeonGreen-BB2 did not co-precipitate with either GFP-TbUnc119 or GFP alone (Fig. 5*B*). Specific interaction between TbArl3A and TbUnc119 was further confirmed by pulldown assays using purified His-TbUnc119 and GST-TbArl3A (Fig. 5, *C* and *D*). Importantly, TbUnc119 did not interact with TbArl13 in the co-immunoprecipitation assays (Fig. 4*A*, also see Fig. 6*C*). This is distinct to the Arl13-Arl3-Unc119 mutual interactions observed in *C. elegans* (25). Additionally, TbUnc119 did not interact with TbArl2 (encoded by Tb927.10.4250) (Fig. S4), which exhibits high sequence similarities to TbArl3A and TbArl3C (29, 44). These interaction results are summarized in Fig. 5*E*.

GTP-locked GST-TbArl3A-Q70L mutant, but not GDP-locked GST-TbArl3A-T30N could pull down His-TbUnc119 (Fig. 6*A*), suggesting that the TbUnc119-TbArl3A interaction is GTP-dependent. This was further validated using nucleotide exchange assays (Fig. 6*B*). Alkaline phosphatase-treated GST-TbArl3A loaded with or without GDP did not interact with His-TbUnc119. GTP-loaded TbArl3A, however, exhibited a strong and specific interaction with TbUnc119.

Our previous studies have shown that TbArl13 acts as a GEF on TbArl3A, as has been reported in mammals (8, 29). We hypothesized that in cells depleted of TbArl13, the level of TbArl3A-GTP in *T. brucei* should decrease, which in turn will affect the interaction between TbUnc119 and TbArl3A. To test this, cells expressing tetracycline-inducible TbArl13-RNAi and cumate-inducible TbUnc119-YFP and TbArl3A-BB2 were generated. Although TbArl3A-BB2 co-immunoprecipitated with TbUnc119-YFP in control cells, their interaction was abolished upon induction of TbArl13-RNAi (Fig. 6*C*). Together, these results demonstrate specific interactions of TbUnc119 with only one of the TbArl3 homologs, TbArl3A, in a GTP-dependent manner, suggesting that TbUnc119 is an effector of TbArl3A that is regulated by TbArl13.

## Discussion

In this study, we revisited the functions of TbUnc119 in light of recent understanding of the LIFT pathway in ciliary biogenesis. Overall our results supported a function of TbUnc119 in flagellar targeting of myristoylated TbAK3. This is consistent with the cargo carrier function of Unc119 observed in mammals and *C. elegans* (11, 24). There are, however, some differences between TbUnc119 and its other eukaryotic counterparts. In *C. elegans,* Unc119 forms mutual interactions with both Arl3 and Arl13, facilitating GTP loading to Arl3. As the interaction between Unc119 and Arl3 is GTP-independent, Unc119 is unlikely an Arl3 effector in *C. elegans* (25). In *T. brucei*, no detectable interaction was observed between TbUnc119 and TbArl13. TbUnc119 interacts with TbArl3A in a GTP-dependent fashion, similar to mammalian Unc119-Arl3 interaction (10, 11). Thus *C. elegans* Unc119 may represent a case of functional divergence, although it appeared more conserved with mammalian Unc119 in the phylogenetic analyses (Fig. S1*A*). One important difference between *T. brucei* and mammalian Unc119 is the lack of TbUnc119-TbArl2 interaction in *T. brucei.* In mammals, Arl2 is shown to interact with Unc119 and displace low-affinity cargoes in the cytosol (10). TbArl2 is essential for cytokinesis in *T. brucei* (44) but this effect is unlikely mediated by TbUnc119 as the depletion of TbUnc119 had no detrimental effects on cell division and viability.

In *T. brucei*, we showed that the binding between TbUnc119 and TbAK3 depended on the myristoylation state of TbAK3.

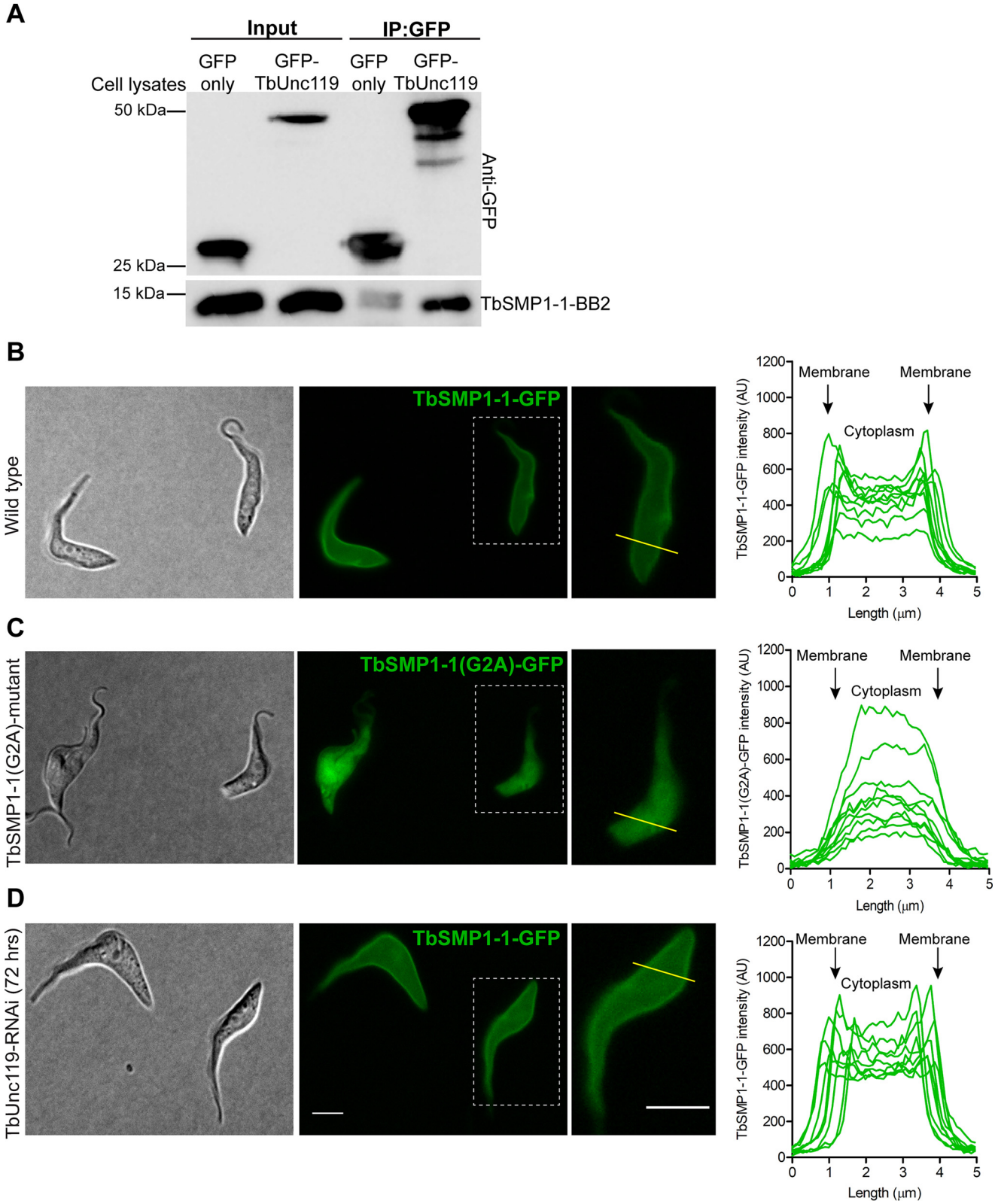


**Figure 4. The cell membrane association of TbSMP1-1 is myristoylation-dependent but TbUnc119-independent.** *A,* TbSMP1-1-BB2 co-immunoprecipitated with GFP-TbUnc119, but not GFP only. *B–D*, cells expressing TbSMP1-1-GFP (*B*) or TbSMP1-1(G2A)-GFP (*C*) were immobilized on agarose gel and imaged live, to best visualize the plasma membrane association of TbSMP1-1-GFP. The intracellular distribution of TbSMP1-1-GFP was also monitored in live cells induced for TbUnc119- RNAi (*D*). All GFP images were collected at constant exposure time. The distribution of TbSMP1-1-GFP in control and TbUnc119-RNAi cells was measured using plot profiling. A line of 5 $\mu$m length was drawn across the entire cell body, encompassing cell membranes at both ends, and fluorescence intensity along the length of this line was plotted. 10 representative cells were shown for control and TbUnc119-RNAi cells. *Insets* show enlarged images of a representative cell from each sample that selected for intensity measurements. *Scale bar*, 5 $\mu$m.

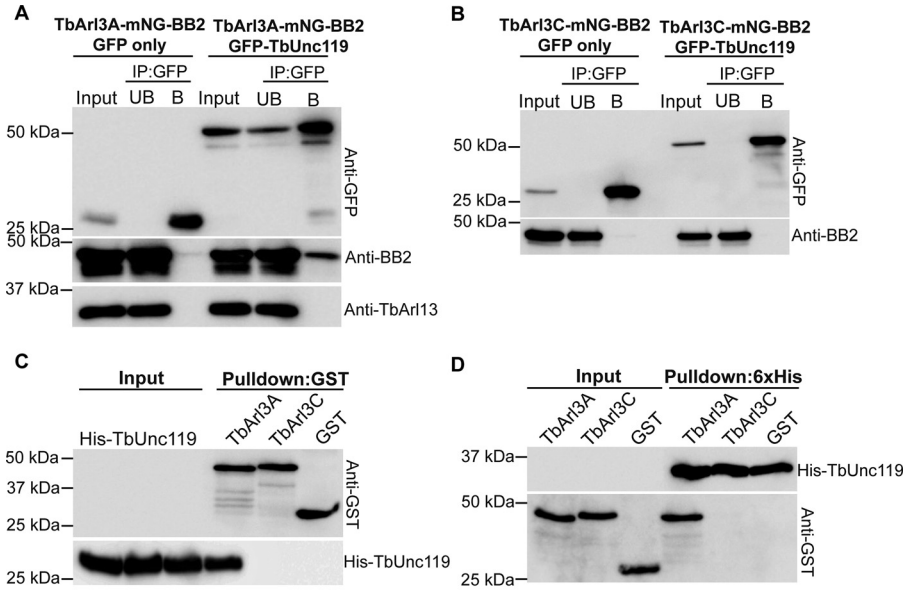


E

| *T. brucei* Arl-GTPases | TbUnc119 | |
|---|---|---|
| | In vivo | In vitro |
| TbArl3A | + | + |
| TbArl3C | - | - |
| TbArl2 | - | - |
| TbArl13 | - | No data |

**Figure 5. TbUnc119 interacts with TbArl3A but not TbArl3C.** *A* and *B, T. brucei* cells co-expressing GFP-TbUnc119 and TbArl3A-mNG-BB2 (*A*) or TbArl3C-mNG-BB2 (*B*) were homogenized, incubated with GFP-nAb beads, and examined for co-immunoprecipitation. Cells expressing GFP only were used as negative controls. *Input*, 5% of cell lysates; *UB*, 5% of unbound fraction; *B*, proteins bound to GFP-nAb beads. *C,* GSH beads coated with GST-TbArl3A, GST-TbArl3C, or GST only were incubated with *E. coli* cell lysates expressing His-TbUnc119. *D,* inverse pulldown using His-TbUnc119-coated beads. *Input*, 12% of cell lysates. *E,* summary of interactions between *T. brucei* Arl-GTPases and TbUnc119.

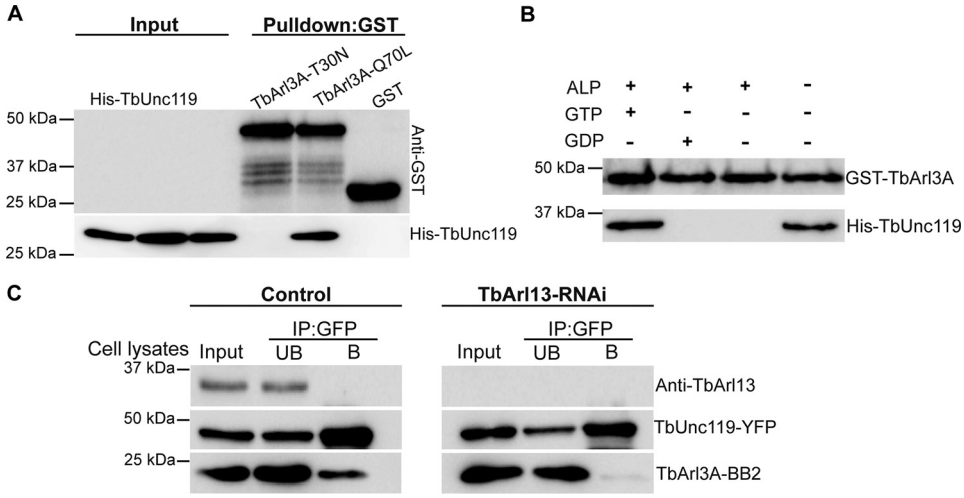


**Figure 6. TbUnc119 interacts with TbArl3A in a GTP-dependent manner.** *A,* GSH beads coated with GST-TbArl3A-T30N, GST-TbArl3A-Q70L, or GST were incubated with bacterial lysates expressing His-TbUnc119. *Input*, 12% of cell lysates. *B,* GST-TbArl3A was treated with or without alkaline phosphatase (*ALP*) and then loaded with GTP or GDP was used to pull down His-TbUnc119. *C,* control and TbArl13-RNAi cells co-expressing TbUnc119-YFP and TbArl3A-BB2 were immunoprecipitated (*IP*) with GFP-nAb beads. TbArl13-RNAi did not affect TbUnc119-YFP and TbArl3ABB2 expression levels, but their binding was abolished. *Input,* 5% of cell lysates; *UB*, 5% of unbound fraction; B: proteins eluted from GFP-nAb beads.

TbUnc119 is able to bind to other myristoylated proteins such as TbSMP1-1, although the function of this binding remained unclear. Depletion of TbUnc119 had no obvious effects on TbSMP1-1 distribution. Considering the lack of growth phenotypes in cultured PCF and BSF cells, depletion of TbUnc119 is unlikely to cause gross perturbation in myristoylated protein distribution or functions, unlike those observed in cells with the myristoylation pathway inhibited (45–47). Depletion of

TbAK3, a flagellar protein identified as TbUnc119 cargo in this study, is also shown to be dispensable for cell growth in culture (38). However, TbAK3-depletion impairs cell motility and parasite infectivity in the tsetse flies (38). TbUnc119 is thus expected to be important for parasite survival in hosts, which remains to be tested. Furthermore, TbUnc119 has many cytoplasmic BioID candidates without predicted myristoylation modification. During the bioinformatic analyses, we could not identify a canonical homologue of PDE6δ, a prenylated cargo carrier, in *T. brucei* and most other single-cellular organisms. Yet protein prenylation and the molecular machinery are clearly present in *T. brucei* (48–50) and several other protists (51). This raised an interesting possibility that TbUnc119 and other protist Unc119 orthologs may be able to carry other lipidated cargoes, particularly prenylated proteins. This possibility should be examined in the future as little is currently known about prenylated targets in *T. brucei*.

A single Arl3 homolog is present in mammals and *C. elegans,* and it is known to interact with and regulate IFT components in addition to its function in displacing cargoes associated with Unc119 (52, 53). *T. brucei* contains three Arl3 homologs. TbArl3A and TbArl3C are highly conserved and syntenic among kinetoplastids, and TbArl3B is diverse with unknown functions (29). Although both TbArl3A and TbArl3C have flagellar functions, only TbArl3A interacted with TbUnc119 and this interaction was regulated by TbArl13. Although it remains to be explored if TbArl3A may have effectors other than TbUnc119, the results support the presence of a conserved LIFT pathway in *T. brucei* that involves TbArl13, TbArl3A, and TbUnc119. Our results also suggest functional diversification and specialization of Arl3-GTPases in *T. brucei.* TbArl3A is localized in the flagellum and the cytoplasm, whereas TbArl3C is restricted to the basal bodies (29). They may function at different subcellular locations on different effectors, which together contribute to the essential phenotypes observed for TbArl13.

## Experimental procedures

### *Bioinformatic analyses*

The amino acid sequences of Unc119 and PDE6δ from various model organisms were obtained from UniProt, Tritrypdb, and NCBI protein database. Multisequence alignments were performed using MUSCLE (54). The output of multisequence alignments was formatted using Multiple Align Show of the Sequence Manipulation Suite (JavaScript application) (55). For phylogenetic analyses, the Unc119 and PDE6δ sequences were aligned using MAFFT (LINSI). ProtTest (version 3.4.2) (56) was used for model selection. Maximum likelihood tree was generated using RAxML (version 8.2.10) and Multiparametric bootstrapping was done using automatic bootstrapping option (autoMRE).

### *Expression constructs, cell culture, and transfections*

All *T. brucei* sequences used in this study were retrieved from the Tritryp database (RRID:SCR_007043). RNAi target sequences were selected using RNAit (57). The details of plasmid constructs used in this study are summarized in Table S3.

The insect proliferative, PCF of *T. brucei* cells were cultured in Cunningham medium supplemented with 10% heat-inactivated fetal bovine serum (FBS; HyClone) at 28 °C. Stable transfection conditions for PCF cells were performed according to previously published protocol (58). 29.13 *T. brucei* cells genetically modified to express T7 RNA polymerase and tetracycline repressor (59) were used to generate the TbUnc119-RNAi cell line. DIpAnt, a PCF *T. brucei* cell line engineered for tetracycline-inducible and cumate-inducible expressions (36) was used to generate stable cell lines for cumate-inducible overexpression and/or tetracycline-induced knockdown experiments. For RNAi in the BSF cells, either a single marker Lister 427 cell line (59) or a double inducible DIb427 cell line (36) was used.

### *Live cell imaging, immunofluorescence, and microscopy*

PCF cells expressing fluorescently tagged proteins were harvested, resuspended in 1× PBS, and spread on the surface of 1% low melting point-agarose gel (Bio-Rad) prepared in conditioned medium. The gel was then placed on an imaging dish with the parasite side facing the coverslip, allowing the cells to be trapped and partially immobilized between the agarose gel and the coverslip. The cells could be imaged at room temperature for at least 30 min or through an entire cell cycle with appropriate temperature and $CO_2$ control (60, 61).

For immunofluorescence assays, *T. brucei* cells expressing fluorescent and/or other epitope tags were washed and resuspended in 1× PBS and attached to coverslips. Cells were fixed with 4% PFA and permeabilized with 0.25% Triton X-100 unless otherwise stated. DNA was stained with DAPI (2.5 μg/ml). Images were captured by Zeiss Axio Observer Z1 fluorescence microscope with a ×63 objective (NA = 1.4) and a CoolSNAP HQ2 CCD camera (Photometrics).

### *Image quantification and statistical analyses*

For quantifications, images acquired using fixed exposure conditions were processed using ImageJ. Fluorescence intensity of the flagellum was performed using the plot profile function, by drawing a 2-$\mu$m line (width = 5 pixels) along the distal overhang of the flagellum, where it is not attached to the cell body. Fluorescence intensity of the cytosol was quantitated over a 2-$\mu$m line (width = 5 pixels) in the posterior region of the cytoplasm away from the kinetoplast and nucleus. The membrane association of TbSMP1-1-GFP or TbSMP1-1(G2A)-GFP proteins was quantitated by plotting a 5-$\mu$m line (width = 1 pixel) transverse the posterior region of the cell body, away from the kinetoplast and nucleus. The fluorescence intensity measurements were plotted on GraphPad Prism 5. The $p$ values were calculated using two-tailed $t$ test with 95% confidence interval.

### *Co-immunoprecipitation and pulldown assays*

0.5-1 × $10^8$ cells co-expressing GFP or GFP-TbUnc119 (induced with 5 μg/ml of cumate for 24 h) and mNeonGreen-BB2–tagged TbArl3-GTPase (29) were harvested by centrifugation at 4500 × $g$ for 7 min at room temperature. After 2 washes with 1× PBS, the cells were resuspended in 1× PBS supplemented with protease inhibitor mixture (Sigma) and homogenized by sonication. The cell lysates were centrifuged at 17,000 × $g$ for 15 min at 4 °C and the cleared supernatants were incubated with magnetic GFP-nAb™ beads (Allele

Biotechnology) to co-precipitate GFP fusion proteins together with their binding partners. Proteins bound to the magnetic beads were eluted by boiling in 1× Laemmli buffer and analyzed by SDS-PAGE and immunoblotting.

GST-tagged TbArl2, TbArl3A, and TbArl3C GTPases and His-TbUnc119 fusion proteins were expressed in *Escherichia coli* (induced with 0.1 mM isopropyl 1-thio-β-D-galactopyranoside). Purification of tagged proteins was performed using nickel-nitrilotriacetic acid beads (Qiagen) or GSH Sepharose™ 4B beads (GE healthcare) according to the manufacturers' instructions. His-TbUnc119 bound to nickel-nitrilotriacetic acid beads were incubated with cell lysates containing GST-TbArl3A, GST-TbArl3C, and GST only. Alternatively, GSH Sepharose™ 4B beads bound to GST or GST fusions including GST-TbArl2 were incubated with His-TbUnc119. Interaction between TbUnc119 and TbArl-GTPases was then examined by SDS-PAGE followed by immunoblotting.

### *Nucleotide exchange assay*

GST-TbArl3A bound to GSH beads was treated with alkaline phosphatase (10 units/ml) to enzymatically dephosphorylate purified GST-TbArl3A (containing a mixture of GTP- or GDP-bound forms) to nascent guanosine state in 1 ml of exchange buffer (20 mM HEPES, pH 7.4, 1 mM $MgCl_2$, 1 mM DTT) supplemented with 50 mM EDTA for 1 h at room temperature. The beads were washed three times with 1 ml of exchange buffer and then incubated with GTP (100 μM), GDP (100 μM), or no nucleotide, in the presence of 100 mM $MgCl_2$ for 1 h at room temperature. Beads were washed once each with exchange buffer and 1× PBS and incubated with purified His-TbUnc119 for 4 h at 4 °C. Beads were then washed three times each with 1% Triton X-100 in 1× PBS followed by 1× PBS. Bound proteins were eluted by boiling in 1× Laemmli buffer and analyzed by immunoblottings.

### *Proximity-dependent biotinylation (BioID) and LC–MS/MS analyses*

Approximately $10^9$ cells were induced for the expression of 3HA-BioID2-TbUnc119 or TbUnc119-BioID2-HA with 5 μg/ml of cumate for 16 h. WT cells were used as negative control. 50 μM biotin was added to each culture 8 h prior to harvest. Cells were washed extensively with PBS, and lysed with lysis buffer (0.4% SDS, 500 mM NaCl, 5 mM EDTA, 1 mM DTT, 50 mM Tris-HCl, pH 7.4) supplemented with protease inhibitors (Sigma). Cell lysates were centrifuged, and the clear supernatant was incubated with streptavidin-coated Dynabeads® (Invitrogen) for 4 h or overnight at 4 °C. The beads were washed twice with PBS containing 1% SDS, twice with PBS containing 1% Triton X-100, and then twice with 1× PBS for 5 min each. The bound proteins were treated with triethylammonium (500 mM, pH 8.5) and reduced with 4 μl of 100 mM Tris(2-carboxyethyl)phosphine at 50 °C for 1 h with gentle mixing. Beads were alkylated with 5 mM MMTS (methyl methanethiosulfonate) at room temperature for 15 min. After overnight on-bead digestion with 2.5 μg of trypsin, peptide fragments were desalted and processed for LC–MS/MS analyses (see Table S1 for details on proteomics sample preparation and data processing procedures). Top candidates identified in 3HA-BioID2-TbUnc119 and TbUnc119-BioID2-HA samples were scanned for the presence of the myristoylation consensus sequence (M*GXXX*S/T) as well as their presence in the previously published myristoylation proteome of *T. brucei* (40).

### *Antibodies for immunostaining and immunoblots*

Anti-HA (1:500; Santa Cruz, sc-7392) and streptavidin-Alexa Fluor 568 (1:2000; Invitrogen) were used in immunofluorescence assays. For immunoblots, anti-YFP (1:1000, rabbit) (62), anti-TbArl13 (1:2000, rabbit) (29), anti-TbBiP (1:1000, rabbit) (63), anti-His (1:5000, mouse; GE Healthcare), anti-GST (1:5000, mouse; Santa Cruz Biotechnology) and anti-BB2 antibodies (1:500, mouse) (43) were used.

## Data availability

The MS proteomics data have been deposited to the ProteomeXchange Consortium via the PRIDE partner repository with the data set identifier PXD019488.

*Acknowledgments*—We thank Dr. Philippe Bastin for the anti-BB2 antibodies, Dr. Yiliu Zhang for the TbUnc119-YFP construct and initial discussions inspiring this work, Dr. Amrita Srivathsan for help with the phylogenetic analyses, Dr. Samuel Dean for the pPOT plasmids for endogenous tagging, and Dr. Prem Prakash Das with proteomics data deposit.

*Author contributions*—M. P. and C. Y. H. conceptualization; M. P. and T. K. L. data curation; M. P. formal analysis; M. P. investigation; M. P. methodology; M. P. and C. Y. H. writing-original draft; M. P., Y. H., and C. Y. H. writing-review and editing; Y. H., T. K. L., and Q. L. resources; C. Y. H. supervision; C. Y. H. funding acquisition; C. Y. H. project administration.

*Funding and additional information*—This work was supported by Singapore Ministry of Education Research Grant MOE2017-T2-2-109.

*Conflict of interest*—The authors declare that they have no conflict of interest with the content of this article.

*Abbreviations*—The abbreviations used are: IFT, intraflagellar transport; LIFT, lipidated protein intraflagellar transport; PDE6**δ**, phosphodiesterase 6**δ**; GEF, guanine nucleotide exchange factor; PCF, procyclic form; BSF, bloodstream form; HA, hemagglutinin; YFP, yellow fluorescent protein; PFA, paraformaldehyde; DAPI, 4′,6-diamidino-2-phenylindole.

## References

1. Reiter, J. F., and Leroux, M. R. (2017) Genes and molecular pathways underpinning ciliopathies. *Nat. Rev. Mol. Cell Biol.* **18,** 533–547 CrossRef Medline
2. Jensen, V. L., and Leroux, M. R. (2017) Gates for soluble and membrane proteins, and two trafficking systems (IFT and LIFT), establish a dynamic ciliary signaling compartment. *Curr. Opin. Cell Biol.* **47,** 83–91 CrossRef Medline
3. Taschner, M., and Lorentzen, E. (2016) The intraflagellar transport machinery. *Cold Spring Harb. Perspect. Biol.* **8,** a028092 CrossRef

4. Prevo, B., Scholey, J. M., and Peterman, E. J. (2017) Intraflagellar transport: mechanisms of motor action, cooperation, and cargo delivery. *FEBS J.* **284,** 2905–2931 CrossRef Medline
5. Lechtreck, K. F. (2015) IFT–cargo interactions and protein transport in cilia. *Trends Biochem. Sci.* **40,** 765–778 CrossRef Medline
6. Ishikawa, H., and Marshall, W. F. (2017) Intraflagellar transport and ciliary dynamics. *Cold Spring Harb. Perspect. Biol.* **9,** a021998 CrossRef
7. Morga, B., and Bastin, P. (2013) Getting to the heart of intraflagellar transport using *Trypanosoma* and *Chlamydomonas* models: the strength is in their differences. *Cilia* **2,** 16 CrossRef Medline
8. Gotthardt, K., Lokaj, M., Koerner, C., Falk, N., Gieël, A., and Wittinghofer, A. (2015) A G-protein activation cascade from Arl13B to Arl3 and implications for ciliary targeting of lipidated proteins. *Elife* **4,** CrossRef
9. Ismail, S. A., Chen, Y. X., Miertzschke, M., Vetter, I. R., Koerner, C., and Wittinghofer, A. (2012) Structural basis for Arl3-specific release of myristoylated ciliary cargo from UNC119. *EMBO J.* **31,** 4085–4094 CrossRef Medline
10. Jaiswal, M., Fansa, E. K., Kosling, S. K., Mejuch, T., Waldmann, H., and Wittinghofer, A. (2016) Novel biochemical and structural insights into the interaction of myristoylated cargo with Unc119 protein and their release by Arl2/3. *J. Biol. Chem.* **291,** 20766–20778 CrossRef Medline
11. Wright, K. J., Baye, L. M., Olivier-Mason, A., Mukhopadhyay, S., Sang, L., Kwong, M., Wang, W., Pretorius, P. R., Sheffield, V. C., Sengupta, P., Slusarski, D. C., and Jackson, P. K. (2011) An ARL3-UNC119-RP2 GTPase cycle targets myristoylated NPHP3 to the primary cilium. *Genes Dev.* **25,** 2347–2360 CrossRef Medline
12. Humbert, M. C., Weihbrecht, K., Searby, C. C., Li, Y., Pope, R. M., Sheffield, V. C., and Seo, S. (2012) ARL13B, PDE6D, and CEP164 form a functional network for INPP5E ciliary targeting. *Proc. Natl. Acad. Sci. U.S.A.* **109,** 19691–19696 CrossRef Medline
13. Ismail, S. A., Chen, Y. X., Rusinova, A., Chandra, A., Bierbaum, M., Gremer, L., Triola, G., Waldmann, H., Bastiaens, P. I., and Wittinghofer, A. (2011) Arl2-GTP and Arl3-GTP regulate a GDI-like transport system for farnesylated cargo. *Nat. Chem. Biol* **7,** 942–949 CrossRef Medline
14. Schwarz, N., Hardcastle, A. J., and Cheetham, M. E. (2012) Arl3 and RP2 mediated assembly and traffic of membrane associated cilia proteins. *Vision Res.* **75,** 2–4 CrossRef Medline
15. Hanke-Gogokhia, C., Wu, Z., Gerstner, C. D., Frederick, J. M., Zhang, H., and Baehr, W. (2016) Arf-like protein 3 (ARL3) regulates protein trafficking and ciliogenesis in mouse photoreceptors. *J. Biol. Chem.* **291,** 7142–7155 CrossRef Medline
16. Veltel, S., Gasper, R., Eisenacher, E., and Wittinghofer, A. (2008) The retinitis pigmentosa 2 gene product is a GTPase-activating protein for Arf-like 3. *Nat. Struct. Mol. Biol.* **15,** 373–380 CrossRef Medline
17. Stephen, L. A., and Ismail, S. (2016) Shuttling and sorting lipid-modified cargo into the cilia. *Biochem. Soc Trans* **44,** 1273–1280 CrossRef Medline
18. Chandra, A., Grecco, H. E., Pisupati, V., Perera, D., Cassidy, L., Skoulidis, F., Ismail, S. A., Hedberg, C., Hanzal-Bayer, M., Venkitaraman, A. R., Wittinghofer, A., and Bastiaens, P. I. (2011) The GDI-like solubilizing factor PDEδa sustains the spatial organization and signalling of Ras family proteins. *Nat. Cell Biol.* **14,** 148–158 CrossRef Medline
19. Cen, O., Gorska, M. M., Stafford, S. J., Sur, S., and Alam, R. (2003) Identification of UNC119 as a novel activator of SRC-type tyrosine kinases. *J. Biol. Chem.* **278,** 8837–8845 CrossRef Medline
20. Lee, Y., Chung, S., Baek, I. K., Lee, T. H., Paik, S. Y., and Lee, J. (2013) UNC119a bridges the transmission of Fyn signals to Rab11, leading to the completion of cytokinesis. *Cell Cycle* **12,** 1303–1315 CrossRef Medline
21. Gorska, M. M., Stafford, S. J., Cen, O., Sur, S., and Alam, R. (2004) Unc119, a novel activator of Lck/Fyn, is essential for T cell activation. *J. Exp. Med.* **199,** 369–379 CrossRef Medline
22. Gorska, M. M., Liang, Q., Karim, Z., and Alam, R. (2009) Uncoordinated 119 protein controls trafficking of Lck via the Rab11 endosome and is critical for immunological synapse formation. *J. Immunol.* **183,** 1675–1684 CrossRef Medline
23. Karim, Z., Vepachedu, R., Gorska, M., and Alam, R. (2010) UNC119 inhibits dynamin and dynamin-dependent endocytic processes. *Cell Signal.* **22,** 128–137 CrossRef Medline
24. Zhang, H., Constantine, R., Vorobiev, S., Chen, Y., Seetharaman, J., Huang, Y. J., Xiao, R., Montelione, G. T., Gerstner, C. D., Davis, M. W., Inana, G., Whitby, F. G., Jorgensen, E. M., Hill, C. P., Tong, L., *et al.* (2011) UNC119 is required for G protein trafficking in sensory neurons. *Nat. Neurosci.* **14,** 874–880 CrossRef Medline
25. Zhang, Q., Li, Y., Zhang, Y., Torres, V. E., Harris, P. C., Ling, K., and Hu, J. (2016) GTP-binding of ARL-3 is activated by ARL-13 as a GEF and stabilized by UNC-119. *Sci. Rep.* **6,** 24534 CrossRef Medline
26. Akiyoshi, B., and Gull, K. (2013) Evolutionary cell biology of chromosome segregation: insights from trypanosomes. *Open Biol.* **3,** 130023 CrossRef Medline
27. Vincensini, L., Blisnick, T., and Bastin, P. (2011) The importance of model organisms to study cilia and flagella biology. *Biologie aujourd'hui* **205,** 5–28 CrossRef Medline
28. Langousis, G., and Hill, K. L. (2014) Motility and more: the flagellum of *Trypanosoma brucei*. *Nat. Rev. Microbiol.* **12,** 505–518 CrossRef Medline
29. Zhang, Y., Huang, Y., Srivathsan, A., Lim, T. K., Lin, Q., and He, C. Y. (2018) The unusual flagellar-targeting mechanism and functions of the trypanosome ortholog of the ciliary GTPase Arl13b. *J. Cell Sci.* **131,** jcs219071 CrossRef
30. Ohshima, S., Ohashi-Suzuki, M., Miura, Y., Yabu, Y., Okada, N., Ohta, N., and Suzuki, T. (2010) TbUNC119 and its binding protein complex are essential for propagation, motility, and morphogenesis of *Trypanosoma brucei* procyclic form cells. *PLoS ONE* **5,** e15577 CrossRef Medline
31. Kim, D. I., Jensen, S. C., Noble, K. A., Kc, B., Roux, K. H., Motamedchaboki, K., and Roux, K. J. (2016) An improved smaller biotin ligase for BioID proximity labeling. *Mol. Biol. Cell* **27,** 1188–1196 CrossRef Medline
32. Roux, K. J., Kim, D. I., Raida, M., and Burke, B. (2012) A promiscuous biotin ligase fusion protein identifies proximal and interacting proteins in mammalian cells. *J. Cell Biol.* **196,** 801–810 CrossRef Medline
33. Constantine, R., Zhang, H., Gerstner, C. D., Frederick, J. M., and Baehr, W. (2012) Uncoordinated (UNC)119: coordinating the trafficking of myristoylated proteins. *Vision Res.* **75,** 26–32 CrossRef Medline
34. Maduro, M., and Pilgrim, D. (1995) Identification and cloning of unc-119, a gene expressed in the *Caenorhabditis elegans* nervous system. *Genetics* **141,** 977–988 Medline
35. Manning, A. G., Crawford, B. D., Waskiewicz, A. J., and Pilgrim, D. B. (2004) unc-119 homolog required for normal development of the zebrafish nervous system. *Genesis* **40,** 223–230 CrossRef Medline
36. Li, F. J., Xu, Z. S., Aye, H. M., Brasseur, A., Lun, Z. R., Tan, K. S. W., and He, C. Y. (2017) An efficient cumate-inducible system for procyclic and bloodstream form *Trypanosoma brucei*. *Mol. Biochem. Parasitol.* **214,** 101–104 CrossRef Medline
37. Dean, S., Sunter, J. D., and Wheeler, R. J. (2017) TrypTag. org: a trypanosome genome-wide protein localisation resource. *Trends Parasitol.* **33,** 80–82 CrossRef Medline
38. Ooi, C. P., Rotureau, B., Gribaldo, S., Georgikou, C., Julkowska, D., Blisnick, T., Perrot, S., Subota, I., and Bastin, P. (2015) The flagellar arginine kinase in *Trypanosoma brucei* is important for infection in tsetse flies. *PLoS ONE* **10,** e0133676 CrossRef Medline
39. Voncken, F., Gao, F., Wadforth, C., Harley, M., and Colasante, C. (2013) The phosphoarginine energy-buffering system of *Trypanosoma brucei* involves multiple arginine kinase isoforms with different subcellular locations. *PLoS ONE* **8,** e65908 CrossRef Medline
40. Wright, M. H., Paape, D., Price, H. P., Smith, D. F., and Tate, E. W. (2016) Global profiling and inhibition of protein lipidation in vector and host stages of the sleeping sickness parasite *Trypanosoma brucei*. *ACS Infect. Dis.* **2,** 427–441 CrossRef Medline
41. Liu, W., Apagyi, K., McLeavy, L., and Ersfeld, K. (2010) Expression and cellular localisation of calpain-like proteins in *Trypanosoma brucei*. *Mol. Biochem. Parasitol.* **169,** 20–26 CrossRef Medline
42. Subota, I., Julkowska, D., Vincensini, L., Reeg, N., Buisson, J., Blisnick, T., Huet, D., Perrot, S., Santi-Rocca, J., Duchateau, M., Hourdel, V., Rousselle, J. C., Cayet, N., Namane, A., Chamot-Rooke, J., *et al.* (2014) Proteomic analysis of intact flagella of procyclic *Trypanosoma brucei* cells identifies novel flagellar proteins with unique sub-localization and dynamics. *Mol. Cell. Proteomics* **13,** 1769–1786 CrossRef Medline

43. Bastin, P., Bagherzadeh, A., Matthews, K. R., and Gull, K. (1996) A novel epitope tag system to study protein targeting and organelle biogenesis in *Trypanosoma brucei*. *Mol. Biochem. Parasitol.* **77,** 235–239 CrossRef Medline
44. Price, H. P., Peltan, A., Stark, M., and Smith, D. F. (2010) The small GTPase ARL2 is required for cytokinesis in *Trypanosoma brucei*. *Mol. Biochem. Parasitol.* **173,** 123–131 CrossRef Medline
45. Frearson, J. A., Brand, S., McElroy, S. P., Cleghorn, L. A. T., Smid, O., Stojanovski, L., Price, H. P., Guther, M. L. S., Torrie, L. S., Robinson, D. A., Hallyburton, I., Mpamhanga, C. P., Brannigan, J. A., Wilkinson, A. J., Hodgkinson, M., *et al.* (2010) *N*-Myristoyltransferase inhibitors as new leads to treat sleeping sickness. *Nature* **464,** 728–732 CrossRef Medline
46. Price, H. P., Güther, M. L. S., Ferguson, M. A., and Smith, D. F. (2010) Myristoyl-CoA:protein *N*-myristoyltransferase depletion in trypanosomes causes avirulence and endocytic defects. *Mol. Biochem. Parasitol.* **169,** 55–58 CrossRef Medline
47. Price, H. P., Menon, M. R., Panethymitaki, C., Goulding, D., McKean, P. G., and Smith, D. F. (2003) Myristoyl-CoA:protein *N*-myristoyltransferase, an essential enzyme and potential drug target in kinetoplastid parasites. *J. Biol. Chem.* **278,** 7206–7214 CrossRef Medline
48. Field, H., Blench, I., Croft, S., and Field, M. C. (1996) Characterisation of protein isoprenylation in procyclic form *Trypanosoma brucei*. *Mol. Biochem. Parasitol.* **82,** 67–80 CrossRef Medline
49. Yokoyama, K., Lin, Y., Stuart, K. D., and Gelb, M. H. (1997) Prenylation of proteins in *Trypanosoma brucei*. *Mol. Biochem. Parasitol.* **87,** 61–69 CrossRef Medline
50. Yokoyama, K., Trobridge, P., Buckner, F. S., Van Voorhis, W. C., Stuart, K. D., and Gelb, M. H. (1998) Protein farnesyltransferase from *Trypanosoma brucei* a heterodimer of 61- and 65-kDa subunits as a new target for antiparasite therapeutics. *J. Biol. Chem.* **273,** 26497–26505 CrossRef Medline
51. Eastman, R. T., Buckner, F. S., Yokoyama, K., Gelb, M. H., and Van Voorhis, W. C. (2006) Thematic review series, lipid posttranslational modifications: fighting parasitic disease by blocking protein farnesylation. *J. Lipid Res.* **47,** 233–240 CrossRef Medline
52. Schwarz, N., Lane, A., Jovanovic, K., Parfitt, D. A., Aguila, M., Thompson, C. L., da Cruz, L., Coffey, P. J., Chapple, J. P., Hardcastle, A. J., and Cheetham, M. E. (2017) Arl3 and RP2 regulate the trafficking of ciliary tip kinesins. *Hum. Mol. Genet.* **26,** 2480–2492 CrossRef Medline
53. Li, Y., Wei, Q., Zhang, Y., Ling, K., and Hu, J. (2010) The small GTPases ARL-13 and ARL-3 coordinate intraflagellar transport and ciliogenesis. *J. Cell Biol.* **189,** 1039–1051 CrossRef Medline
54. Edgar, R. C. (2004) MUSCLE: multiple sequence alignment with high accuracy and high throughput. *Nucleic Acids Res.* **32,** 1792–1797 CrossRef Medline
55. Stothard, P. (2000) The sequence manipulation suite: JavaScript programs for analyzing and formatting protein and DNA sequences. *BioTechniques* **28,** 1102–1104 CrossRef
56. Darriba, D., Taboada, G. L., Doallo, R., and Posada, D. (2011) ProtTest 3: fast selection of best-fit models of protein evolution. *Bioinformatics* **27,** 1164–1165 CrossRef Medline
57. Field, S. R. S., Vadivelu, J., and Mark, C. (2003) RNAit: an automated web-based tool for the selection of RNAi targets in *Trypanosoma brucei*. *Mol. Biochem. Parasitol.* **128,** 115–118 CrossRef Medline
58. Beverley, S. M., and Clayton, C. E. (1993) Transfection of *Leishmania* and *Trypanosoma brucei* by electroporation. in *Protocols in Molecular Parasitology* (Hyde, J. E., ed) pp. 333–348, Humana Press, Totowa, NJ
59. Wirtz, E., Leal, S., Ochatt, C., and Cross, G. M. (1999) A tightly regulated inducible expression system for conditional gene knock-outs and dominant-negative genetics in *Trypanosoma brucei*. *Mol. Biochem. Parasitol.* **99,** 89–101 CrossRef Medline
60. He, C. Y., Ho, H. H., Malsam, J., Chalouni, C., West, C. M., Ullu, E., Toomre, D., and Warren, G. (2004) Golgi duplication in *Trypanosoma brucei*. *J. Cell Biol.* **165,** 313–321 CrossRef Medline
61. He, C. Y., Singh, A., and Yurchenko, V. (2019) Cell cycle-dependent flagellar disassembly in a firebug Trypanosomatid *Leptomonas pyrrhocoris*. *mBio* **10,** CrossRef
62. Gheiratmand, L., Brasseur, A., Zhou, Q., and He, C. Y. (2013) Biochemical characterization of the bi-lobe reveals a continuous structural network linking the bi-lobe to other single-copied organelles in *Trypanosoma brucei*. *J. Biol. Chem.* **288,** 3489–3499 CrossRef Medline
63. Bangs, J. D., Uyetake, L., Brickman, M. J., Balber, A. E., and Boothroyd, J. C. (1993) Molecular cloning and cellular localization of a BiP homologue in *Trypanosoma brucei*: divergent ER retention signals in a lower eukaryote. *J. Cell Sci.* **105,** 1101–1113